



32 To simulate iodine-initiated NPF (I-NPF) in controlled laboratory conditions, I_2 or CH_2I_2 vapor
33 was usually photolyzed in the presence of ozone to provide nucleation precursors (Burkholder et al.,
34 2004; Jimenez et al., 2003; Monahan et al., 2012; Saunders and Plane, 2005; O’ Dowd et al., 2004;
35 Martín et al., 2020; He et al., 2021; Huang et al., 2022). Ashu-Ayem et al. (2012); Monahan et al.
36 (2012); Mcfiggans et al. (2004); Sellegri et al. (2005) and Sellegri et al. (2016) also investigated the
37 NPF from the vapors emitted by real-world macroalgal specimens or seawater in laboratory chamber
38 or apparatus. However, the focus of all above studies are emission rate, oxidation mechanisms or
39 nucleation pathways of iodine species. For example, positive correlations between particle
40 concentrations and I_2 or CH_2I_2 mixing ratios were usually observed (Burkholder et al., 2004; Jimenez
41 et al., 2003; Sellegri et al., 2005; Monahan et al., 2012). Kinetic studies in flow tube or CERN
42 CLOUD chamber proposed the clustering of iodine oxides (I_xO_y) or iodine oxoacids (HIO_3 , HIO_2) as
43 nucleation mechanisms on the basis of photoionization TOF-MS (Martín et al., 2020), Api-TOF and
44 nitrate-Chemical Ionization Mass Spectrometer (CIMS) measurements (He et al., 2021). A recent
45 chamber study showed heterogeneous reaction between iodine oxide nanoparticle, meso-erythritol
46 (or glyoxal) and dimethylamine accelerated nanoparticle growth (Huang et al., 2022).

47 Until now, no prior work has investigated the exact chemical identity of organic compounds
48 (other than iodinated methane) and their role in I-NPF. The role of biogenic terpenes and
49 anthropogenic aromatics in continental NPF has been recognized for a long time (Donahue et al.,
50 2013). Their ozonolysis or photochemistry products have been investigated in depth by using
51 Electrospray Ionization Mass Spectrometry (ESI-MS) and more recently, CIMS (Nguyen et al., 2010;
52 Kundu et al., 2017; Kundu et al., 2012; Faxon et al., 2018; Wang et al., 2020; Riva et al., 2017; Yan
53 et al., 2020; Ehn et al., 2014). It is very likely that certain volatile organic compounds (VOCs)
54 emitted mutually with iodine or iodinated methane from coastal biota or biologically active sea
55 surface may also be involved in coastal I-NPF process and promote the growth of iodine particles.

56 To test this hypothesis, we conducted oxidation and NPF experiments with vapor emissions from
57 real-world coastal macroalgae in a bag reactor. A suite of mass spectrometric methods including
58 Inductively Coupled Plasma-MS (ICP-MS), Gas Chromatography-MS (GC-MS), iodide-CIMS and
59 ESI-orbitrap MS were applied to measure vapor precursors, gaseous products and particulate
60 products during the NPF process. Mass concentrations of total organic carbon (TOC) and total iodine
61 (TI) of new particles were compared to evaluate the relative importance of organics and iodine in
62 new particle growth. The identity and transformation mechanisms of organic compounds were
63 identified to provide a more complete story of coastal NPF from low-tide macroalgal emission. Our
64 study is thus complementary to prior laboratory and field studies of I-NPF, but has an emphasis on



65 organics.

66 2. Experiments

67 2.1 Experimental apparatus and sample collection

68 Similar to Potential Aerosol Mass (PAM) Oxidation Flow Reactor, a bag reactor was designed to
69 provide an oxidizing environment for simulating atmospheric oxidation processes of algae-emitted
70 VOCs. The bag reactor was made from 75 μm -thick fluorinated ethylene propylene (FEP) Teflon
71 (1.2 m \times 1.5 m, flat dimension). The volume of the bag at full inflation was determined
72 experimentally to be about 200 L. The bag was suspended vertically (Figure 1) and kept in the dark
73 or directly exposed to room light of fluorescent lamp. Because the purpose of this study is to
74 qualitatively measure the oxidation products of algae-emitted VOCs, wall loss, production rate and
75 other kinetic factors in the bag reactor were not evaluated. Fresh macroalgae (*Undaria pinnatifida*)
76 was collected from intertidal zone at Xiangshan gulf of east China coast and stored at -10 °C until the
77 experiments. 2 kg macroalgae was put in a 20 L Pyrex glass bottle that was filled with ~1 L natural
78 seawater. The specimens was partially exposed to the air to simulate tidal emersion of macroalgae. A
79 flow of particle-free ultra high purity (UHP) air blew algae-emitted VOCs out of the bottle and
80 merged with a diluting air flow before entering the bag reactor.

81 Two types of experiments were conducted. In the three ozonolysis experiments, ozone (O_3) was
82 generated by flowing an UHP air flow through a 5 Watts 185 nm UV lamp. The O_3 flow was fed just
83 before the bag reactor was fully inflated. Final O_3 concentration in the bag reactor was measured to
84 be ~200 ppbv using an ozone analyzer (Model 49i, Thermo-Fisher Scientific Inc.). In an additional
85 OH-enhanced experiment, the O_3 /VOC mixture flow was directed through a 254 nm UV light before
86 entering the bag reactor. OH radicals were produced via the reaction $\text{O}_3+h\nu\rightarrow\text{O}_2+\text{O}(^1\text{D})$ and
87 $\text{O}(^1\text{D})+\text{H}_2\text{O}\rightarrow 2\text{OH}$.

88 Before each experiment, the bag was purged for several hours to reduce background particle
89 concentrations to below 1 cm^{-3} . The bag reactor was first operated in a static mode to monitor the
90 time evolution of gaseous products and particle size, and then in a dynamic mode to collect enough
91 particles for offline chemical analysis. In the static mode, the bag was first filled to full inflation with
92 the VOCs/ O_3 flows. The flows were then shut down; a Scanning Mobility Particle Sizer (SMPS,
93 model 3936, TSI Inc., Shoreview, MN, USA) and an Aerodyne iodide-CIMS pulled two flows of 0.3
94 liters per minute (lpm) and 1.8 lpm out of the bag, respectively. The SMPS measured the particle
95 number size distribution from 14 to 600 nm.



96 In the dynamic mode, the VOCs/O₃ flow of 3 lpm was fed to the bag continuously, while the
97 SMPS and a vacuum pump (GAST Group Ltd.) pulled sample flows of 0.3 and 2.7 lpm, respectively,
98 out of the bag reactor. This resulted in an overall residential time of 67 minutes for the O₃/VOC
99 mixture in the fully inflated bag. The particles in the 2.7 lpm sample flow were collected onto a
100 Zefluor® PTFE membrane filter mounted in a filter inlet for gases and aerosols (FIGAERO) for
101 iodide-CIMS analysis, or alternatively, onto 47 mm diameter double quartz fiber filter pack mounted
102 in a filter holder for ESI-orbitrap MS, ICP-MS and TOC analysis. The front filter of the double filter
103 pack collected the particles, while the back filter placed downstream of the front filter was supposed
104 to adsorb the same amount of volatile species as the front filter.

105 **2.2 Chemical analysis**

106 Before the ozonolysis experiments, the algae-emitted VOCs in the bag reactor was collected by a
107 6-liter pre-evacuated stainless-steel canisters (Entech Instruments, Inc., Simi Valley, CA, USA) and
108 was analyzed using a quadrupole GC-MS system (model TH-300B, Wuhan Tianhong Instruments Co.
109 Ltd., Wuhan, China). The algae-emitted VOCs, as well as their gaseous and particulate products,
110 were also measured by the FIGAERO-iodide-CIMS. Iodide-adduct chemical ionization is well suited
111 for measuring oxygenated or acidic compounds with minimal fragmentation. More details of the
112 GC-MS and FIGAERO-iodide-CIMS measurements can be found in Supporting Material. The
113 theory and design of the two instruments were described by Wang et al. (2014) and Lopez-Hilfiker et
114 al. (2014).

115 The particles collected on quartz fiber filters were sent for offline quantification of TOC and TI,
116 as well as non-target analysis of organic compounds using ESI-orbitrap MS. The front and back
117 filters were treated, separately, following the procedure as below: the filter was ultrasonicated twice
118 with 10-mL water and acetone nitrile solvent mixture (v:v=1:1). The extract was filtered by a 0.2 µm
119 PTFE syringe filter and evaporated in a rotary evaporator to 0.5 mL. After being centrifuged for 30
120 min at 12000 rpm, the supernatant was collected for TI analysis by Agilent 1100 HPLC-7900
121 ICP-MS (Agilent Technologies, Santa Clara, CA, USA) and TOC analysis by a TOC analyzer
122 (Model TOC-5000A, Shimadzu, Japan). TI or TOC in the particles was obtained by subtracting the
123 amount on the back filter from that on the front filter. Nontarget analysis of organic compounds in
124 the supernatant was conducted using a Q Exactive hybrid Quadrupole-Orbitrap mass spectrometer
125 (Thermo Scientific, Bremen, Germany). The supernatant was directly infused by a syringe pump and
126 ionized in negative ESI source. All the ions in the m/z range from 50 to 500 Th were scanned with a
127 mass resolution of 70000. The chemically sound CHO molecular formulas were computed with a



128 mass tolerance of ± 2 ppm for these ions. Only the compounds that existed solely in the front filter or
129 with ion intensity in the front filter higher than that in the back filter by a factor of 3 were regarded
130 as the organic compounds in the particle phase.

131 **3. Results and discussion**

132 **3.1 Relative mass contribution of organic carbon and iodine to new particles**

133 Typical banana-shape particle size spectrum observed in the static mode of an ozonolysis
134 experiment is shown in Figure 2a. In the presence of room light, new particles larger than 14 nm
135 were observed only 58 minutes after the injection of ozone flow. This relative long time is due to the
136 build-up of O_3 concentration and subsequent accumulation of oxidation products. No particles were
137 formed in the absence of room light or ozone. In the dynamic mode experiments, O_3 in the bag
138 reactor was kept at its maximum concentration 200 ppbv. With a prolonged residential time of 67
139 min, the particles grew to 102 ± 23 nm, which was measured by the SMPS at the outlet of the bag
140 reactor. The TOC and TI measurements show that organic compounds contributed more particle
141 mass than iodine with TOC/(I+TOC) ratio of $96.1 \pm 2.9\%$ (Table 1).

142 In the OH-enhanced experiment (dynamic mode), more particulate products were generated with
143 enhanced oxidation capacity: TI in the particles increased by a factor of 10.8; TOC increased by a
144 factor of 2.7; particle number concentration increased by a factor of 7.4. On the other hand, particle
145 size decreased to 73 nm and TOC/(TI+TOC) ratio decreased to 92.9% (Table 1). These differences
146 indicate that more iodine nuclei were produced with enhanced OH concentration, probably via
147 $OIO+OH \rightarrow HOIO_2$ (Plane et al., 2006). Competitive uptake of condensing organic vapors onto these
148 iodine nuclei limited the growth of individual new particles. Nevertheless, organic compounds
149 overwhelmingly dominated over iodine in the mass contribution to new particle growth.

150 The significant organic contribution observed in the laboratory condition is generally consistent
151 with TOC/(I+TOC) ratio of 98.2% in 10-56 nm new particles collected during a coastal I-NPF event in
152 China (Yu et al., 2019), although TOC and TI during the field event are two orders of magnitude
153 lower than those in the bag reactor (Table 1). Mean diameter of new particles was observed to be
154 only 16 nm during the field event. But those small new particles are expected to grow into CCN
155 active sizes, given longer residence time and uptake of more condensing vapors in the atmosphere.

156 **3.2 Macroalgal emission**

157 It is of particular interest to know what VOCs are emitted from coastal macroalgae. They are



158 potential precursors of iodine particle nucleation and growth. The canister sampling followed by
159 GC-MS analysis showed that the top 9 non-CHO compounds with highest TIC peak areas (Table 2)
160 are C₅ alkanes, C₁₀ alpha-pinene and halogenated C₁, C₃ and C₅ alkanes. The top 10 CHO
161 compounds are C₂-C₆ alcohols and carbonyls with saturated or unsaturated carbon chain.

162 Iodide-CIMS is more sensitive to more oxygenated or acidic compounds and thus complementary
163 to the GC-MS measurement. The 76 organic precursors detected by iodide-CIMS before ozone
164 addition were characterized by C_{1,2,3,6} and O_{2,3} formulas (Figure 3a). The top 7 compounds with
165 highest ion intensities were CH₂O₂, C₂H₄O₂, C₃H₆O₃, C₆H₁₀O₃, C₂H₆O₂, C₄H₈O₂ and C₆H₁₂O₃,
166 which accounted for 82.5% of total ion intensity. They are C₁-C₆ mono-carboxylic acids, hydroxyl
167 carboxylic acids or oxo-carboxylic acids with 2 to 3 oxygen atoms (Table 2). Their carbon atom
168 numbers are in general consistent with the VOCs detected by GC-MS.

169 Relatively high signals of HNO₃ were observed as NO₃⁻ and HNO₃I⁻ before the addition of ozone
170 to the bag reactor. Because HNO₃ and HNO₂ were also observed as deprotonated ions or I⁻ clusters in
171 the particle phase during the NPF, HNO₃ is also an important precursor of particle formation.

172 3.3 Gaseous and particulate products

173 3.3.1 Inorganic molecules and radicals

174 Being different from nitrate-CIMS, our iodide-CIMS did not detect nucleating clusters of iodine
175 oxides or oxyacids after the addition of ozone. Instead, dozens of new inorganic molecules or
176 radicals were observed as clusters with I⁻, NO₃⁻ or deprotonated ions in the gas or particle phase
177 (Figure 4). We grouped these species by elemental composition and investigated their role in the
178 NPF by observing how their gaseous ion intensities evolved during the NPF event in the bag reactor
179 (Figure 2b-2f).

180 1. Cl, I, Cl₂ and ClI in the gas phase: the intensities of I and Cl increased ca. 10 minutes before 14
181 nm particles appeared and decreased as the particles grew up. Based on prior work of Burkholder et
182 al. (2004); Jimenez et al. (2003); O'dowd et al. (2004), we suggested the photolysis of CH₂Cl₂,
183 CHBrCl, CH₃I and C₃H₇I was the source of halogen atoms (e.g., CH₃I+hν→CH₃+I). There was a
184 time lag of 20-25 minutes between the appearances of Cl and I and those of ClI and Cl₂, which were
185 probably from the recombination of Cl and I atoms.

186 2. IO₂, IO, ClIO, INO₂ and ClNO₂ in the gas phase: these species showed a similar time series to I
187 and Cl atoms. IO, IO₂ and ClIO could be from the reactions between I, ClI and O₃. INO₂ is usually
188 thought to form upon the reaction I+NO₂+M→INO₂+M (Saiz-Lopez et al., 2012). ClNO₂ was likely



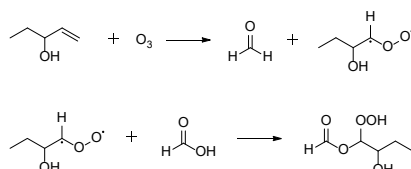
189 to form upon similar reaction between Cl and NO₂ in the bag reactor.

190 3. HIO₃ and INO₃: the two species seem to be the end products of above intermediates, because
191 their intensities kept on increasing during new particle growth. INO₃, which is iodine nitrate IONO₂,
192 was detected in both gas and particle phases. IONO₂ probably formed upon the recombination of IO
193 and NO₂ (IO+NO₂+M→IONO₂+M) (Saiz-Lopez et al., 2012). HIO₃ was likely to form via
194 OIO+OH→HOIO₂ or I + H₂O + O₃→HOIO₂ + OH (Plane et al., 2006; Martín et al., 2020). HIO₃
195 was not detected in particle phase by iodide-CIMS, which is contrary to the observation by
196 HPLC-ICP-MS that total iodine was mostly dominated IO₃⁻ peak. The signals of IO⁻, IO₂⁻ and
197 HIONO₃⁻ in the particle phase are therefore most likely to result from thermal decomposition of
198 HIO₃ to HIO and HIO₂ in the FIGAERO thermal desorption process.

199 4. CH₃SO₃H, S₂⁻, S₃⁻, SO₃⁻: We observed methane sulfonic acid (CH₃SO₃H, MSA) in both gas and
200 particle phases. Gaseous MSA increased in the beginning, but decreased after new particles appeared
201 (Figure 2f). Apparently, our measurement suggested MSA contributed to the growth of new particles,
202 but it is unknown if it also participated in nucleation. We suggested S₂⁻, S₃⁻, SO₃⁻ ions observed in the
203 particle phase were thermal decomposition products of MSA.

204 3.3.2 Gaseous organic products

205 After ozone addition, a gradual transformation from C₁-C₃ precursors to C₅-C₈ gaseous products
206 was observed during the NPF process (Figure 2h). In the meanwhile, the oxygen atom number of the
207 compounds increased from 2-3 to 4-7 (Figure 2g). The formation of compounds with more carbon
208 atoms than the parent VOCs is unlikely in the gas phase, except bimolecular reactions of stabilized
209 Criegee intermediates (SCIs) that typically form upon alkene ozonolysis. Similar to isoprene
210 ozonolysis (Riva et al., 2017; Inomata et al., 2014), we propose the SCI addition mechanism can
211 also explain the transformation observed in our case: (1) C₄ SCIs formed upon the ozonolysis of
212 CHO precursors with C=C double bonds (e.g., those observed by GC-MS in Table 2). (2) the
213 insertion of C₄ SCIs into carboxylic acid precursors (e.g., those observed by CIMS in Table 2)
214 produced oligomeric hydroperoxides. An example was shown in Scheme I for the reactions of most
215 abundant ethyl vinyl carbinol (C₅H₁₀O), ozone and formic acid (CH₂O₂), but the same mechanism is
216 also applicable for ethyl vinyl ketone (C₅H₈O) and other abundant C₂-C₅ carboxylic acids and
217 hydroxyl carboxylic acids. As a result, a series of gaseous oligomeric hydroperoxides C₅H₁₀O₅,
218 C₆H₁₀O₅, C₆H₁₂O₅, C₇H₁₂O₆, C₇H₁₄O₆, C₈H₁₄O₅, C₈H₁₆O₆, C₈H₁₆O₅ and C₉H₁₆O₆ were observed with
219 high intensity by iodide-CIMS.



Scheme I

221 3.3.3 Particulate organic products

222 In the end of a typical ozonolysis experiment (dynamic mode), 100 and 364 new formulas were
223 observed in the gas and particle phases, respectively, including 73 semi-VOCs appeared in both gas
224 and particle phases. Those semi-VOCs accounted for 81 and 20% of total ion intensities of gaseous
225 and particulate products, respectively. Being different from unimodal atom number distributions of
226 gaseous products ($C_{\max}=7$ and $O_{\max}=5$, Figure 3b), particulate products were characterized by
227 distinct bimodal or trimodal distribution of carbon number ($C_{\max}=8, 14$ and 16 , Figure 3c) and
228 oxygen number ($O_{\max}=4$ and 8), implying possible dimer formation via accretion reactions in the
229 particle phase.

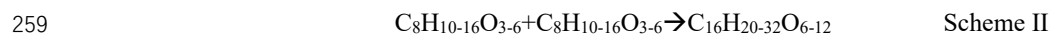
230 ESI-Orbitrap MS differs from FIGAERO-iodide-CIMS in extraction method (ultrasonic solvent
231 extraction from quartz fiber filter vs. thermal desorption from PTFE membrane filter), ionization
232 source (electrospray ionization vs. iodide-adduct chemical ionization) and MS resolving power
233 (70000 vs. 4500). The result showed that ESI-orbitrap MS and FIGAERO-iodide-CIMS detected 336
234 and 364 organic formulas, respectively, in the particle phase. 167 organic formulas were commonly
235 observed by both methods, which accounted for 87% and 54% of total ion intensity of organic
236 formulas by the two methods, respectively (Figure S1). As shown in Figure 3c and 3d,
237 FIGAERO-iodide-CIMS had better sensitivity toward the organic compounds with more oxygen
238 atoms (e.g., $O \geq 8$) and carbon atoms (e.g., $C \geq 10$). As a result, bimodal carbon and oxygen atom
239 number distributions were observed by FIGAERO-iodide-CIMS, but not ESI-orbitrap MS.

240 The measurement by ESI-orbitrap MS provided more insights about the formation mechanism of
241 particulate products. We compared the 336 formulas detected by ESI-orbitrap MS in our study with
242 the 414 formulas of isoprene ozonolysis SOA products (Nguyen et al., 2010) and 922 formulas of
243 alpha-pinene ozonolysis SOA products (Putman et al., 2012) measured by the ESI-orbitrap MS. It
244 was found that 72% of the formulas in this study can also be found in isoprene SOA, but only 39%
245 can be found in alpha-pinene SOA. This seems to imply that some similar alkene ozonolysis
246 reactions occurred in our system and isoprene ozonolysis.

247 For such a highly complex system full of various algae-emitted precursors, it is impossible to



248 simply propose a reaction mechanism to explain the formation of all particulate products, nor to list
249 all reactions occurring in the bag reactor. On the basis of particle-phase oligomer chemistry (Seinfeld
250 and Pandis, 2016), especially the well-understood isoprene ozonolysis SOA chemistry (Nguyen et al.,
251 2010; Inomata et al., 2014; Riva et al., 2017), we suggest a variety of accretion reactions without
252 uniform oligomerization pattern (e.g., esterification, aldol condensation, hemiacetal reactions,
253 peroxyhemiacetal formation and SCI reactions, etc.) transformed $O_{\max}=4$ and $C_{\max}=8$ multifunctional
254 monomers (like alcohols, carbonyls, hydroperoxides, carboxylic acids) to $O_{\max}=8$ and $C_{\max}=14$ or 16
255 dimers. Scheme II illustrated addition type self- and cross-oligomerization between C_6 and C_8
256 monomers produces C_{14} and C_{16} dimers. All the formulas in Scheme II are among the most abundant
257 ones observed in the particle phase by the iodide-CIMS.



260 **4. Conclusions**

261 Using a suite of mass spectrometers, we reported, for the first time, the chemical compositions of
262 volatile precursors emitted by real-world coastal macroalgae and their gaseous and particulate
263 oxidation products. In the presence of room light and ozone, the photolysis of halogenated $C_{1,3,5}$
264 alkanes ends up as HIO_3 and INO_3 . It was most likely HIO_3 initiated NPF and provided nuclei for the
265 further condensation of other products like INO_3 , MSA and CHO compounds. Gas-phase SCI
266 reactions and particle-phase accretion reactions transformed C_1 - C_6 and O_2 - O_3 precursors gradually to
267 particulate products with $C_{\max}=8, 14$ and 16 and $O_{\max}=4$ and 8. As a result, organic carbon were
268 found to overwhelmingly dominated over iodine in the mass contribution to the new particle growth.
269 Although our instruments did not allow the detection of nucleating clusters of iodine oxides or
270 oxyacids, our study provided important complementary information to the ongoing laboratory and
271 field researches of coastal I-NPF.

272 **Data Availability**

273 All data related to figures and tables in this study are archived and made available through
274 Zenodo data repository <https://doi.org/10.5281/zenodo.6965859>.

275 **Financial support.**

276 This work was supported by the National Science Foundation of China (grant no. 41975831 and
277 42175131) and Start-up research funding from China University of Geosciences.



278 **Competing Interests.**

279 The authors declare that they have no conflict of interest.

280 **Author contributions**

281 HY designed the experiment. YW, XH and CX conducted the experiments. YW and HY analyzed
282 the data and wrote the manuscript. QW and XG reviewed and revised the manuscript.

283 **References**

- 284 Allan, J. D., Williams, P. I., Najera, J., Whitehead, J. D., Flynn, M. J., Taylor, J. W., Liu, D.,
285 Darbyshire, E., Carpenter, L. J., Chance, R., Andrews, S. J., Hackenberg, S. C., and McFiggans,
286 G.: Iodine observed in new particle formation events in the Arctic atmosphere during ACCACIA,
287 *Atmos. Chem. Phys.*, 15, 5599-5609, <https://doi.org/10.5194/acp-15-5599-2015>, 2015.
- 288 Ashu-Ayem, E. R., Nitschke, U., Monahan, C., Chen, J., Darby, S. B., Smith, P. D., O'Dowd, C. D.,
289 Stengel, D. B., and Venables, D. S.: Coastal Iodine Emissions. 1. Release of I₂ by *Laminaria*
290 *digitata* in Chamber Experiments, *Environmental Science & Technology*, 46, 10413-10421,
291 <https://doi.org/10.1021/es204534v>, 2012.
- 292 Baccarini, A., Karlsson, L., Dommen, J., Duplessis, P., Vüllers, J., Brooks, I. M., Saiz-Lopez, A.,
293 Salter, M., Tjernström, M., Baltensperger, U., Zieger, P., and Schmale, J.: Frequent new particle
294 formation over the high Arctic pack ice by enhanced iodine emissions, *Nature Communications*,
295 11, 4924, <https://doi.org/10.1038/s41467-020-18551-0>, 2020.
- 296 Beck, L. J., Sarnela, N., Junninen, H., Hoppe, C. J. M., Garmash, O., Bianchi, F., Riva, M., Rose, C.,
297 Peräkylä, O., Wimmer, D., Kausiala, O., Jokinen, T., Ahonen, L., Mikkilä, J., Hakala, J., He, X.-C.,
298 Kontkanen, J., Wolf, K. K. E., Cappelletti, D., Mazzola, M., Traversi, R., Petroselli, C., Viola, A.
299 P., Vitale, V., Lange, R., Massling, A., Nøjgaard, J. K., Krejci, R., Karlsson, L., Zieger, P., Jang, S.,
300 Lee, K., Vakkari, V., Lampilahti, J., Thakur, R. C., Leino, K., Kangasluoma, J., Duplissy, E.-M.,
301 Siivola, E., Marbouti, M., Tham, Y. J., Saiz-Lopez, A., Petäjä, T., Ehn, M., Worsnop, D. R., Skov,
302 H., Kulmala, M., Kerminen, V.-M., and Sipilä, M.: Differing Mechanisms of New Particle
303 Formation at Two Arctic Sites, *Geophysical Research Letters*, 48, e2020GL091334,
304 <https://doi.org/10.1029/2020GL091334>, 2021.
- 305 Burkholder, J. B., Curtius, J., Ravishankara, A. R., and Lovejoy, E. R.: Laboratory studies of the
306 homogeneous nucleation of iodine oxides, *Atmospheric Chemistry and Physics*, 4, 19-34,
307 <https://doi.org/10.5194/acp-4-19-2004>, 2004.
- 308 Donahue, N. M., Ortega, I. K., Chuang, W., Riipinen, I., Riccobono, F., Schobesberger, S., Dommen,



- 309 J., Baltensperger, U., Kulmala, M., Worsnop, D. R., and Vehkamäki, H.: How do organic vapors
310 contribute to new-particle formation?, *Faraday Discussions*, 165, 91-104,
311 <https://doi.org/10.1039/C3FD00046J>, 2013.
- 312 Ehn, M., Thornton, J. A., Kleist, E., Sipila, M., Junninen, H., Pullinen, I., Springer, M., Rubach, F.,
313 Tillmann, R., Lee, B., Lopez-Hilfiker, F., Andres, S., Acir, I.-H., Rissanen, M., Jokinen, T.,
314 Schobesberger, S., Kangasluoma, J., Kontkanen, J., Nieminen, T., Kurten, T., Nielsen, L. B.,
315 Jorgensen, S., Kjaergaard, H. G., Canagaratna, M., Maso, M. D., Berndt, T., Petaja, T., Wahner, A.,
316 Kerminen, V.-M., Kulmala, M., Worsnop, D. R., Wildt, J., and Mentel, T. F.: A large source of
317 low-volatility secondary organic aerosol, *Nature*, 506, 476-479,
318 <https://doi.org/10.1038/nature13032>, 2014.
- 319 Faxon, C., Hammes, J., Le Breton, M., Pathak, R. K., and Hallquist, M.: Characterization of organic
320 nitrate constituents of secondary organic aerosol (SOA) from nitrate-radical-initiated oxidation of
321 limonene using high-resolution chemical ionization mass spectrometry, *Atmospheric Chemistry
322 and Physics*, 18, 5467-5481, <https://doi.org/10.5194/acp-18-5467-2018>, 2018.
- 323 He, X. C., Tham, Y. J., Dada, L., Wang, M., Finkenzeller, H., Stolzenburg, D., Iyer, S., Simon, M.,
324 Kurten, A., Shen, J., Rorup, B., Rissanen, M., Schobesberger, S., Baalbaki, R., Wang, D. S.,
325 Koenig, T. K., Jokinen, T., Sarnela, N., Beck, L. J., Almeida, J., Amanatidis, S., Amorim, A., Ataei,
326 F., Baccharini, A., Bertozzi, B., Bianchi, F., Brilke, S., Caudillo, L., Chen, D., Chiu, R., Chu, B.,
327 Dias, A., Ding, A., Dommen, J., Duplissy, J., El Haddad, I., Gonzalez Carracedo, L., Granzin, M.,
328 Hansel, A., Heinritzi, M., Hofbauer, V., Junninen, H., Kangasluoma, J., Kempainen, D., Kim, C.,
329 Kong, W., Krechmer, J. E., Kvashin, A., Laitinen, T., Lamkaddam, H., Lee, C. P., Lehtipalo, K.,
330 Leiminger, M., Li, Z., Makhmutov, V., Manninen, H. E., Marie, G., Marten, R., Mathot, S.,
331 Mauldin, R. L., Mentler, B., Mohler, O., Muller, T., Nie, W., Onnela, A., Petaja, T., Pfeifer, J.,
332 Philippov, M., Ranjithkumar, A., Saiz-Lopez, A., Salma, I., Scholz, W., Schuchmann, S., Schulze,
333 B., Steiner, G., Stozhkov, Y., Tauber, C., Tome, A., Thakur, R. C., Vaisanen, O., Vazquez-Pufleau,
334 M., Wagner, A. C., Wang, Y., Weber, S. K., Winkler, P. M., Wu, Y., Xiao, M., Yan, C., Ye, Q.,
335 Ylisirnio, A., Zauner-Wieczorek, M., Zha, Q., Zhou, P., Flagan, R. C., Curtius, J., Baltensperger,
336 U., Kulmala, M., Kerminen, V. M., Kurten, T., Donahue, N. M., Volkamer, R., Kirkby, J.,
337 Worsnop, D. R., and Sipila, M.: Role of iodine oxoacids in atmospheric aerosol nucleation,
338 *Science*, 371, 589-595, <https://doi.org/10.1126/science.abe0298>, 2021.
- 339 Heard, D. E., Read, K. A., Methven, J., Al-Haider, S., Bloss, W. J., Johnson, G. P., Pilling, M. J.,
340 Seakins, P. W., Smith, S. C., Sommariva, R., Stanton, J. C., Still, T. J., Ingham, T., Brooks, B., De
341 Leeuw, G., Jackson, A. V., McQuaid, J. B., Morgan, R., Smith, M. H., Carpenter, L. J., Carslaw,
342 N., Hamilton, J., Hopkins, J. R., Lee, J. D., Lewis, A. C., Purvis, R. M., Wevill, D. J., Brough, N.,



- 343 Green, T., Mills, G., Penkett, S. A., Plane, J. M. C., Saiz-Lopez, A., Worton, D., Monks, P. S.,
344 Fleming, Z., Rickard, A. R., Alfarra, M. R., Allan, J. D., Bower, K., Coe, H., Cubison, M., Flynn,
345 M., McFiggans, G., Gallagher, M., Norton, E. G., O'Dowd, C. D., Shillito, J., Topping, D.,
346 Vaughan, G., Williams, P., Bitter, M., Ball, S. M., Jones, R. L., Povey, I. M., O'Doherty, S.,
347 Simmonds, P. G., Allen, A., Kinnersley, R. P., Beddows, D. C. S., Dall'Osto, M., Harrison, R. M.,
348 Donovan, R. J., Heal, M. R., Jennings, S. G., Noone, C., and Spain, G.: The North Atlantic Marine
349 Boundary Layer Experiment(NAMBLEX). Overview of the campaign held at Mace Head, Ireland,
350 in summer 2002, *Atmos. Chem. Phys.*, 6, 2241-2272, 10.5194/acp-6-2241-2006, 2006.
- 351 Huang, R.-J., Hoffmann, T., Ovadnevaite, J., Laaksonen, A., Kokkola, H., Xu, W., Xu, W., Ceburnis,
352 D., Zhang, R., Seinfeld, J. H., and O'Dowd, C.: Heterogeneous iodine-organic chemistry
353 fast-tracks marine new particle formation, *Proceedings of the National Academy of Sciences*, 119,
354 e2201729119, <https://doi.org/10.1073/pnas.2201729119>, 2022.
- 355 Inomata, S., Sato, K., Hirokawa, J., Sakamoto, Y., Tanimoto, H., Okumura, M., Tohno, S., and
356 Imamura, T.: Analysis of secondary organic aerosols from ozonolysis of isoprene by proton
357 transfer reaction mass spectrometry, *Atmospheric Environment*, 97, 397-405,
358 <https://doi.org/10.1016/j.atmosenv.2014.03.045>, 2014.
- 359 Jimenez, J. L., Bahreini, R., Cocker III, D. R., Zhuang, H., Varutbangkul, V., Flagan, R. C., Seinfeld,
360 J. H., O'Dowd, C. D., and Hoffmann, T.: New particle formation from photooxidation of
361 diiodomethane (CH₂I₂), *Journal of Geophysical Research: Atmospheres*, 108,
362 <https://doi.org/10.1029/2002JD002452>, 2003.
- 363 Kundu, S., Fisseha, R., Putman, A. L., Rahn, T. A., and Mazzoleni, L. R.: High molecular weight
364 SOA formation during limonene ozonolysis: insights from ultrahigh-resolution FT-ICR mass
365 spectrometry characterization, *Atmos. Chem. Phys.*, 12, 5523-5536,
366 <https://doi.org/10.5194/acp-12-5523-2012>, 2012.
- 367 Kundu, S., Fisseha, R., Putman, A. L., Rahn, T. A., and Mazzoleni, L. R.: Molecular formula
368 composition of β -caryophyllene ozonolysis SOA formed in humid and dry conditions,
369 *Atmospheric Environment*, 154, 70-81, <https://doi.org/10.1016/j.atmosenv.2016.12.031>, 2017.
- 370 Lopez-Hilfiker, F. D., Mohr, C., Ehn, M., Rubach, F., Kleist, E., Wildt, J., Mentel, T. F., Lutz, A.,
371 Hallquist, M., Worsnop, D., and Thornton, J. A.: A novel method for online analysis of gas and
372 particle composition: description and evaluation of a Filter Inlet for Gases and AEROSols
373 (FIGAERO), *Atmospheric Measurement Techniques*, 7, 983-1001,
374 <https://doi.org/10.5194/amt-7-983-2014>, 2014.
- 375 Martín, J. C. G., Lewis, T. R., Blitz, M. A., Plane, J. M. C., Kumar, M., Francisco, J. S., and
376 Saiz-Lopez, A.: A gas-to-particle conversion mechanism helps to explain atmospheric particle



- 377 formation through clustering of iodine oxides, *Nature Communications*, 11, 4521,
378 <https://doi.org/10.1038/s41467-020-18252-8>, 2020.
- 379 McFiggans, G., Coe, H., Burgess, R., Allan, J., Cubison, M., Alfarra, M. R., Saunders, R.,
380 Saiz-Lopez, A., Plane, J. M. C., Wevill, D., Carpenter, L., Rickard, A. R., and Monks, P. S.: Direct
381 evidence for coastal iodine particles from *Laminaria* macroalgae – linkage to emissions of
382 molecular iodine, *Atmos. Chem. Phys.*, 4, 701-713, <https://doi.org/10.5194/acp-4-701-2004>, 2004.
- 383 McFiggans, G., Bale, C. S. E., Ball, S. M., Beames, J. M., Bloss, W. J., Carpenter, L. J., Dorsey, J.,
384 Dunk, R., Flynn, M. J., Furneaux, K. L., Gallagher, M. W., Heard, D. E., Hollingsworth, A. M.,
385 Hornsby, K., Ingham, T., Jones, C. E., Jones, R. L., Kramer, L. J., Langridge, J. M., Leblanc, C.,
386 LeCrane, J. P., Lee, J. D., Leigh, R. J., Longley, I., Mahajan, A. S., Monks, P. S., Oetjen, H.,
387 Orr-Ewing, A. J., Plane, J. M. C., Potin, P., Shillings, A. J. L., Thomas, F., von Glasow, R., Wada,
388 R., Whalley, L. K., and Whitehead, J. D.: Iodine-mediated coastal particle formation: an overview
389 of the Reactive Halogens in the Marine Boundary Layer (RHAMBLE) Roscoff coastal study,
390 *Atmospheric Chemistry and Physics*, 10, 2975-2999, <https://doi.org/10.5194/acp-10-2975-2010>,
391 2010.
- 392 Monahan, C., Ashu-Ayem, E. R., Nitschke, U., Darby, S. B., Smith, P. D., Stengel, D. B., Venables,
393 D. S., and O'Dowd, C. D.: Coastal Iodine Emissions: Part 2. Chamber Experiments of Particle
394 Formation from *Laminaria digitata*-Derived and Laboratory-Generated I₂, *Environmental Science*
395 *& Technology*, 46, 10422-10428, <https://doi.org/10.1021/es3011805>, 2012.
- 396 Nguyen, T. B., Bateman, A. P., Bones, D. L., Nizkorodov, S. A., Laskin, J., and Laskin, A.:
397 High-resolution mass spectrometry analysis of secondary organic aerosol generated by ozonolysis
398 of isoprene, *Atmospheric Environment*, 44, 1032-1042,
399 <https://doi.org/10.1016/j.atmosenv.2009.12.019>, 2010.
- 400 O'Dowd, C. D., Jimenez, J. L., Bahreini, R., Flagan, R. C., Seinfeld, J. H., Hämeri, K., Pirjola, L.,
401 Kulmala, M., Jennings, S. G., and Hoffmann, T.: Marine aerosol formation from biogenic iodine
402 emissions, *Nature*, 417, 632, <https://doi.org/10.1038/nature00775>, 2002.
- 403 O'Dowd, C. D., Facchini, M. C., Cavalli, F., Cebrunis, D., Mircea, M., Decesari, S., Fuzzi, S., Yoon,
404 Y. J., and Putard, J.-P.: Biogenically driven organic contribution to marine aerosol, *Nature*, 431,
405 676-680, <https://doi.org/10.1038/nature02959>, 2004.
- 406 Plane, J. M. C., Joseph, D. M., Allan, B. J., Ashworth, S. H., and Francisco, J. S.: An Experimental
407 and Theoretical Study of the Reactions OIO + NO and OIO + OH, *The Journal of Physical*
408 *Chemistry A*, 110, 93-100, <https://doi.org/10.1021/jp055364y>, 2006.
- 409 Putman, A. L., Offenberg, J. H., Fisseha, R., Kundu, S., Rahn, T. A., and Mazzoleni, L. R.:
410 Ultrahigh-resolution FT-ICR mass spectrometry characterization of α -pinene ozonolysis SOA,



- 411 Atmospheric Environment, 46, 164-172, <https://doi.org/10.1016/j.atmosenv.2011.10.003>, 2012.
- 412 Riva, M., Budisulistiorini, S. H., Zhang, Z. F., Gold, A., Thornton, J. A., Turpin, B. J., and Surratt, J.
413 D.: Multiphase reactivity of gaseous hydroperoxide oligomers produced from isoprene ozonolysis
414 in the presence of acidified aerosols, Atmospheric Environment, 152, 314-322,
415 <https://doi.org/10.1016/j.atmosenv.2016.12.040>, 2017.
- 416 Saiz-Lopez, A., Plane, J. M. C., Baker, A. R., Carpenter, L. J., von Glasow, R., Gómez Martín, J. C.,
417 McFiggans, G., and Saunders, R. W.: Atmospheric Chemistry of Iodine, Chemical Reviews, 112,
418 1773-1804, <https://doi.org/10.1021/cr200029u>, 2012.
- 419 Saunders, R. W. and Plane, J. M. C.: Formation Pathways and Composition of Iodine Oxide
420 Ultra-Fine Particles, Environmental Chemistry, 2, 299-303, <https://doi.org/10.1071/EN05079>,
421 2005.
- 422 Seinfeld, J. H. and Pandis, S. N.: Atmospheric chemistry and physics: from air pollution to climate
423 change, 3rd, John Wiley and Sons. Inc., New York, 2016.
- 424 Sellegri, K., Yoon, Y. J., Jennings, S. G., O'Dowd, C. D., Pirjola, L., Cautenet, S., Chen, H., and
425 Hoffmann, T.: Quantification of Coastal New Ultra-Fine Particles Formation from In situ and
426 Chamber Measurements during the BIOFLUX Campaign, Environmental Chemistry, 2, 260-270,
427 <https://doi.org/10.1071/EN05074>, 2005.
- 428 Sellegri, K., Pey, J., Rose, C., Culot, A., DeWitt, H. L., Mas, S., Schwier, A. N., Temime-Roussel, B.,
429 Charriere, B., Saiz-Lopez, A., Mahajan, A. S., Parin, D., Kukui, A., Sempere, R., D'Anna, B., and
430 Marchand, N.: Evidence of atmospheric nanoparticle formation from emissions of marine
431 microorganisms, Geophysical Research Letters, 43, 6596-6603,
432 <https://doi.org/10.1002/2016GL069389>, 2016.
- 433 Sipilä, M., Sarnela, N., Jokinen, T., Henschel, H., Junninen, H., Kontkanen, J., Richters, S.,
434 Kangasluoma, J., Franchin, A., Peräkylä, O., Rissanen, M. P., Ehn, M., Vehkamäki, H., Kurten, T.,
435 Berndt, T., Petäjä, T., Worsnop, D., Ceburnis, D., Kerminen, V.-M., Kulmala, M., and O'Dowd, C.:
436 Molecular-scale evidence of aerosol particle formation via sequential addition of HIO₃, Nature,
437 537, 532-534, <https://doi.org/10.1038/nature19314>, 2016.
- 438 Wang, M., Zeng, L., Lu, S., Shao, M., Liu, X., Yu, X., Chen, W., Yuan, B., Zhang, Q., Hu, M., and
439 Zhang, Z.: Development and validation of a cryogen-free automatic gas chromatograph system
440 (GC-MS/FID) for online measurements of volatile organic compounds, Analytical Methods, 6,
441 9424-9434, <https://doi.org/10.1039/C4AY01855A>, 2014.
- 442 Wang, M., Chen, D., Xiao, M., Ye, Q., Stolzenburg, D., Hofbauer, V., Ye, P., Vogel, A. L., Mauldin, R.
443 L., 3rd, Amorim, A., Baccarini, A., Baumgartner, B., Brilke, S., Dada, L., Dias, A., Duplissy, J.,
444 Finkenzeller, H., Garmash, O., He, X. C., Hoyle, C. R., Kim, C., Kvashnin, A., Lehtipalo, K.,



445 Fischer, L., Molteni, U., Petäjä, T., Pospisilova, V., Quéléver, L. L. J., Rissanen, M., Simon, M.,
446 Tauber, C., Tomé, A., Wagner, A. C., Weitz, L., Volkamer, R., Winkler, P. M., Kirkby, J., Worsnop,
447 D. R., Kulmala, M., Baltensperger, U., Dommen, J., El-Haddad, I., and Donahue, N. M.:
448 Photo-oxidation of Aromatic Hydrocarbons Produces Low-Volatility Organic Compounds,
449 *Environmental science & technology*, 54, 7911-7921, <https://doi.org/10.1021/acs.est.0c02100>,
450 2020.

451 Whitehead, J. D., McFiggans, G. B., Gallagher, M. W., and Flynn, M. J.: Direct linkage between
452 tidally driven coastal ozone deposition fluxes, particle emission fluxes, and subsequent CCN
453 formation, *Geophysical Research Letters*, 36, <https://doi.org/10.1029/2008GL035969>, 2009.

454 Yan, C., Nie, W., Vogel, A. L., Dada, L., Lehtipalo, K., Stolzenburg, D., Wagner, R., Rissanen, M. P.,
455 Xiao, M., Ahonen, L., Fischer, L., Rose, C., Bianchi, F., Gordon, H., Simon, M., Heinritzi, M.,
456 Garmash, O., Roldin, P., Dias, A., Ye, P., Hofbauer, V., Amorim, A., Bauer, P. S., Bergen, A.,
457 Bernhammer, A. K., Breitenlechner, M., Brilke, S., Buchholz, A., Mazon, S. B., Canagaratna, M.
458 R., Chen, X., Ding, A., Dommen, J., Draper, D. C., Duplissy, J., Frege, C., Heyn, C., Guida, R.,
459 Hakala, J., Heikkinen, L., Hoyle, C. R., Jokinen, T., Kangasluoma, J., Kirkby, J., Kontkanen, J.,
460 Kürten, A., Lawler, M. J., Mai, H., Mathot, S., Mauldin, R. L., 3rd, Molteni, U., Nichman, L.,
461 Nieminen, T., Nowak, J., Ojdanic, A., Onnela, A., Pajunoja, A., Petäjä, T., Piel, F., Quéléver, L. L.
462 J., Sarnela, N., Schallhart, S., Sengupta, K., Sipilä, M., Tomé, A., Tröstl, J., Väisänen, O., Wagner,
463 A. C., Ylisirniö, A., Zha, Q., Baltensperger, U., Carslaw, K. S., Curtius, J., Flagan, R. C., Hansel,
464 A., Riipinen, I., Smith, J. N., Virtanen, A., Winkler, P. M., Donahue, N. M., Kerminen, V. M.,
465 Kulmala, M., Ehn, M., and Worsnop, D. R.: Size-dependent influence of NO(x) on the growth
466 rates of organic aerosol particles, *Science advances*, 6, eaay4945,
467 <https://doi.org/10.1126/sciadv.aay4945>, 2020.

468 Yu, H., Ren, L., Huang, X., Xie, M., He, J., and Xiao, H.: Iodine speciation and size distribution in
469 ambient aerosols at a coastal new particle formation hotspot in China, *Atmospheric Chemistry and
470 Physics*, 19, 4025-4039, <https://doi.org/10.5194/acp-19-4025-2019>, 2019.

471

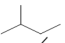
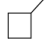
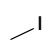
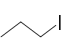
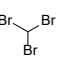
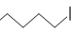
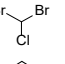
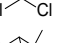

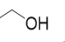
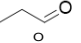
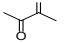
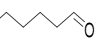
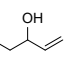
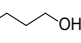
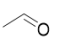
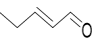
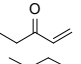
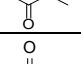
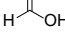
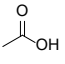
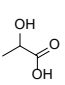
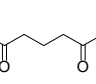
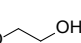
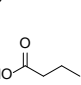


Table 1. Particle number concentration (N), mean diameter (D_p), total organic carbon (TOC) and total iodine (TI) of new particles with a residential time of 67 min in the bag reactor in the ozonolysis experiments and OH-enhanced experiment (dynamic mode). Those of 10-56 nm new particles collected by a nano Micro-Orifice Uniform Deposit Impactor (nano-MOUDI, MSP, Inc.) during an I-NPF event at a coastal site of Ningbo, China (Yu *et al.*, 2019) were also listed.

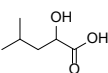
	TOC ($\mu\text{g m}^{-3}$)	TI ($\mu\text{g m}^{-3}$)	TOC/(TI+TOC)	N (cm^{-3})	D_p (nm)
ozonolysis experiments	45.6±9.7	0.88±0.34	96.1±2.9%	$(5.58±2.04)\times 10^4$	102±23
OH-enhanced experiment	125.3	9.5	92.9%	4.16×10^5	73
I-NPF event at a coastal site of China	0.7	0.0135	98.2%	6.00×10^5	16



Table 2. Major volatile organic compounds emitted by macroalgae as potential NPF precursors, sorted by TIC peak area measured by GC/MS or MS peak intensity measured by iodide-CIMS

	Formula	Structure	Peak area/MS peak intensity
1	C ₅ H ₁₂		1.90×10 ⁶
2	C ₅ H ₁₀		1.59×10 ⁶
3	CH ₃ I		1.37×10 ⁶
4	C ₃ H ₇ I		7.60×10 ⁵
5	CHBr ₃		4.71×10 ⁵
6	C ₅ H ₁₁ I		3.75×10 ⁵
7	CHBr ₂ Cl		2.71×10 ⁵
8	CH ₂ Cl ₂		2.55×10 ⁵
9	C ₁₀ H ₁₆		2.26×10 ⁵
1	C ₂ H ₆ O		1.70×10 ⁷
2	C ₃ H ₆ O		1.38×10 ⁷
3	C ₄ H ₆ O ₂		1.30×10 ⁷
4	C ₆ H ₁₂ O		1.03×10 ⁷
5	C ₅ H ₁₀ O		1.00×10 ⁷
6	C ₄ H ₁₀ O		5.16×10 ⁷
8	C ₂ H ₄ O		3.46×10 ⁷
9	C ₆ H ₁₀ O		2.88×10 ⁷
7	C ₅ H ₈ O		1.45×10 ⁷
10	C ₄ H ₈ O		1.37×10 ⁷
1	CH ₂ O ₂		1.58×10 ⁶
2	C ₂ H ₄ O ₂		9.52×10 ⁵
3	C ₃ H ₆ O ₃		9.21×10 ⁵
4	C ₆ H ₁₀ O ₃		4.44×10 ⁵
5	C ₂ H ₆ O ₂		2.88×10 ⁵
6	C ₄ H ₈ O ₂		1.17×10 ⁵



7	$C_6H_{12}O_3$		1.12×10^5
---	----------------	---	--------------------

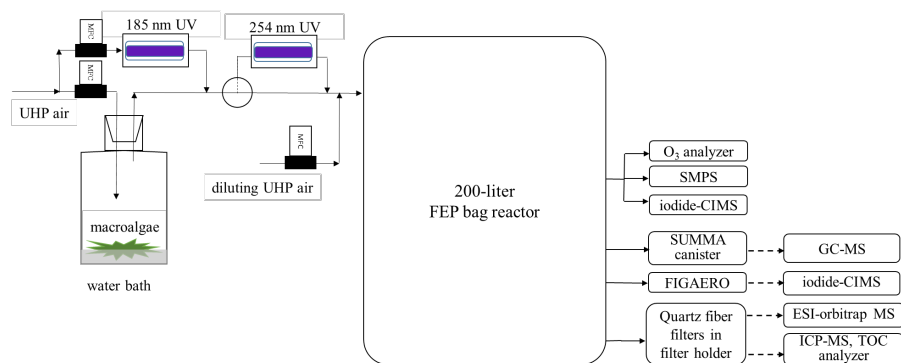


Figure 1. Schematic of experimental setup. Solid line: air flows. Dashed lines: sent for offline chemical analysis.

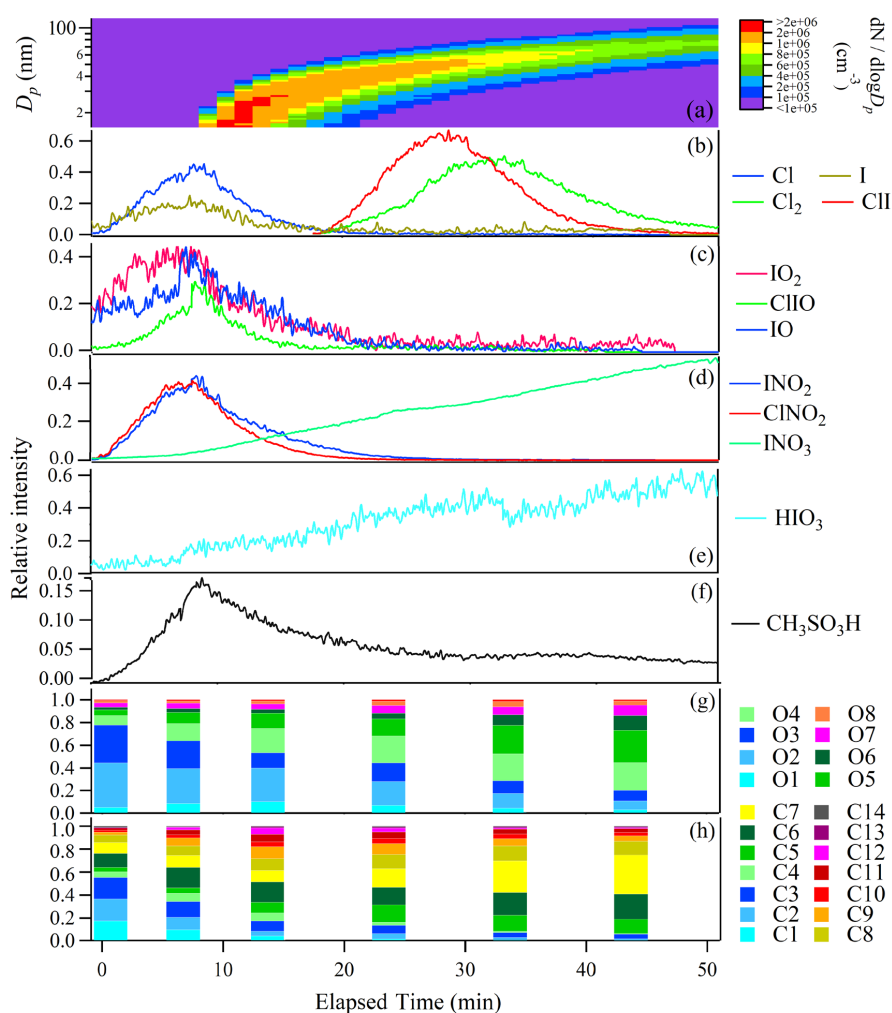


Figure 2. Time evolution of particle number size distribution (a) and relative intensities of gaseous molecules and radicals (b-f); the fractions of organic compounds grouped by O and C atom numbers in the selected time points (g-h) in a typical ozonolysis experiment (static mode). Time zero was chosen as the start time when HIO₃ was observed.

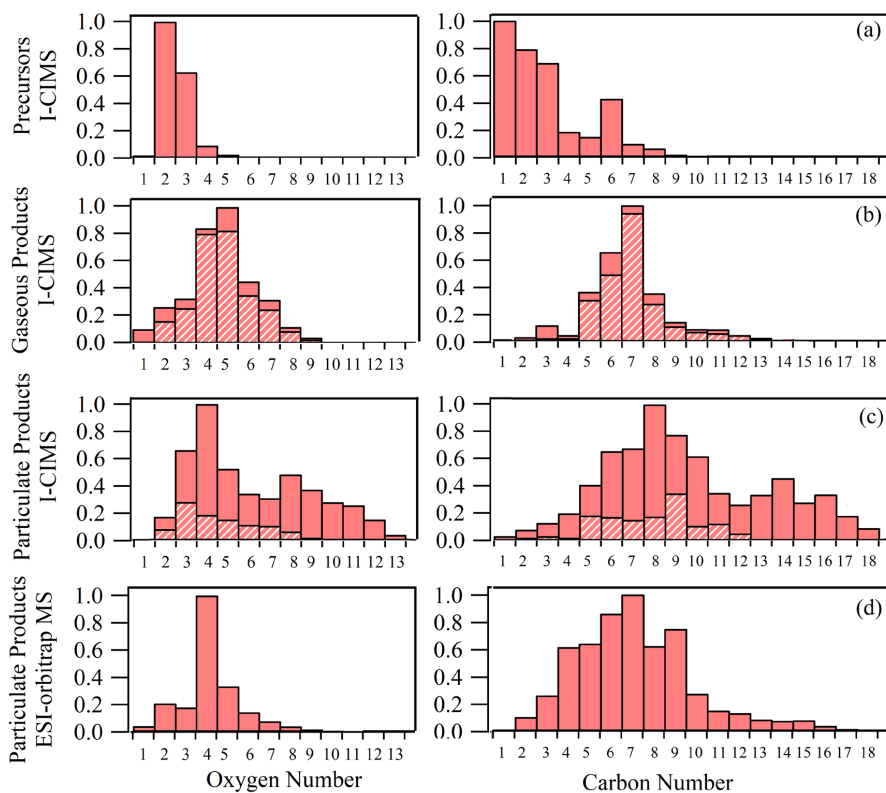


Figure 3. Oxygen and carbon atom number distributions of potential VOC precursors (a), gaseous products (b) and particulate products measured by iodide-CIMS (c), as well as the particulate products measured by ESI-orbitrap MS (d) in a typical ozonolysis experiment (dynamic mode). Hatched bars indicate the fractions of organic formulas observed in both gas and particle phases by iodide-CIMS.

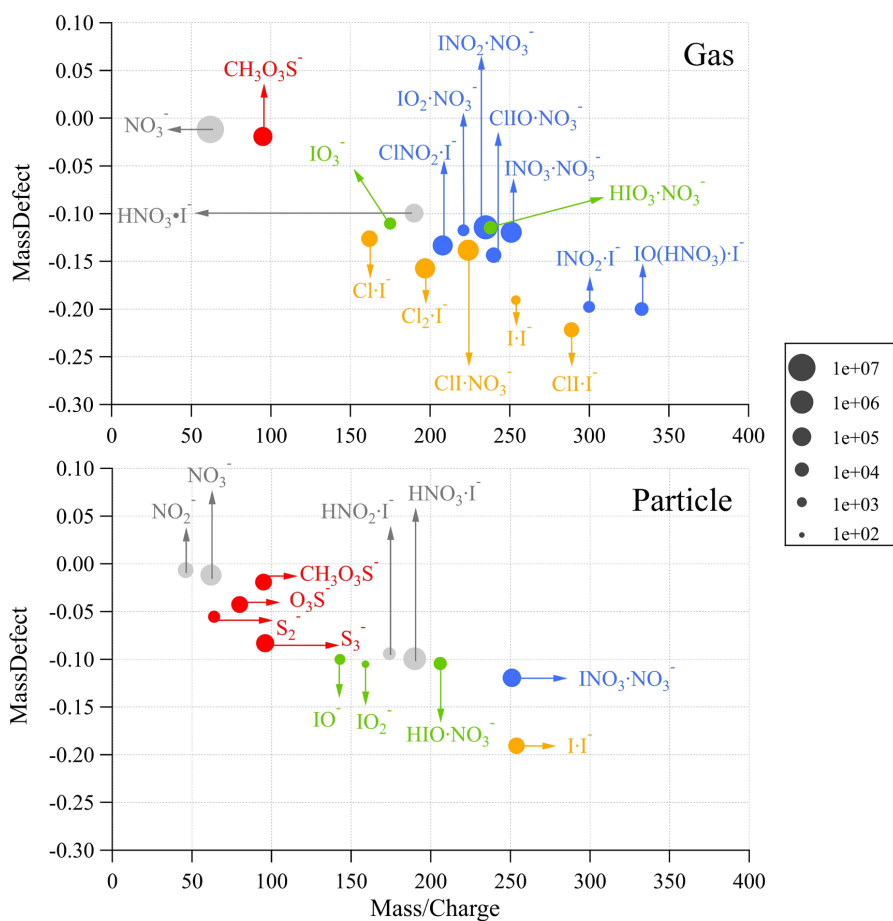


Figure 4. Integrated ion intensities of inorganic molecules and radicals in the gas phase (static mode) and particle phase (dynamic mode) measured by iodide-CIMS in a typical ozonolysis experiment. The ions were coded in color according to their elemental composition